*Journal of Metals, Materials and Minerals, 34(3), 1963, 2024*

# Vibration absorption of as-built and post-heat-treated Ti-6Al-4V alloy fabricated by laser powder bed fusion additive manufacturing

Masaaki NAKAI[1,*], Kohei NAGAYA[1], Kosuke UEKI[1], and Hideki KYOGOKU[2]

[1] *Graduate School of Science and Engineering, Kindai University, 3-4-1 Kowakae, Higashiosaka, Osaka 577-8502, Japan*
[2] *Fundamental Technology for Next Generation Research Institute, Kindai University, 1 Takaya Umenobe, Higashihiroshima, Hiroshima 739-2116, Japan*

***Corresponding author e-mail**: nakai@mech.kindai.ac.jp

**Received date:**
17 February 2024
**Revised date:**
25 March 2024
**Accepted date:**
18 August 2024

**Keywords:**
Additive manufacturing;
Ti-6Al-4V;
Vibration absorption;
Anisotropy;
Post-heat treatment

**Abstract**

Vibration absorption of the Ti-6Al-4V alloy fabricated by laser powder bed fusion additive manufacturing (LPBF-AM) was evaluated following as-built and post-heat treatment (i.e., solution treatment followed by water quenching). The base plate was heated at 50°C or 200°C during building. Results showed that the vibration absorption of the as-built Ti-6Al-4V alloy was higher when the base plate was heated at 50°C than at 200°C. Further, the vibration absorption indicated strong anisotropy, with the highest vibration absorption in the direction perpendicular to the building direction and transverse to the laser scanning direction. However, after solution treatment followed by water quenching, the anisotropy in the vibration absorption of the LPBF-AMed Ti-6Al-4V alloy practically disappeared, and relatively high values were obtained parallel to each direction.

## 1. Introduction

The Ti-6Al-4V alloy is used as a structural material for artificial satellites. Satellite components are often too complex in shape to enable the efficient placement of various onboard devices, and the production number is small because of the considerable cost of a single launch. In recent years, additive manufacturing (AM) technologies using metals [1] have been employed to manufacture satellite components [2]. AM technology enables the manufacture of hollow structures, which is not possible with machining, and individual manufacturing. Therefore, reductions in the weight of components and manufacturing costs are expected. Satellites are sometimes destroyed or malfunction because of vibrations and explosions (violent vibrations of air) caused by engine jets when launched by rockets [3]. The natural frequency of a typical satellite is less than 30 Hz, and high-frequency vibrations exceeding 100 Hz from the attachment point are damped in the vibration transmission path, whereas an explosion noise of 130 dB or more, mainly from several hundred hertz to several kilohertz from any angle during launch, causes large vibrations in the satellite structure [4]. Therefore, the use of highly vibrational absorbers for satellite components is desirable.

The logarithmic damping rate is generally used as a measure of vibration absorbency. This is correlated and proportional to the internal friction of the material. The internal friction of metallic materials is affected by lattice defects, such as dislocations and point defects [5], depending on the history of plastic working, heat treatment, and impurity concentration. Titanium alloys exhibit significantly lower vibrational absorption properties than other metallic materials [6]. However, studies have shown that a solution treatment at a temperature in the single β region, following by quenching, increased internal friction of α+β-type Ti-Nb binary alloys due to martensitic transformation and then significantly improved the vibration absorption [7,8]. The Ti-6Al-4V alloy is also an α+β-type titanium alloy, and thus martensitic transformation can be induced by solution treatment at 1100°C or higher, followed by water quenching. This is likely to result in improved vibration absorption. Among the AM technologies using metals, laser powder bed fusion (LPBF) is one of the most representative methods. It is known that LPBF exhibits the following features, (a) a steep temperature gradient ($10^6$ K·m$^{-1}$) as well as rapid solidification and cooling rates (can reach $10^8$ K·s$^{-1}$) and (b) a complex heat history involving melting and solidification as well as multiple reheating and cooling cycles for solidified parts [9]. Therefore, according to both the (a) and (b) effects, a microstructure containing a hierarchical structure of martensite was obtained in the LPBF-AMed Ti-6Al-4V alloy [9,10]. Such the microstructure is difficult to be obtained without LPBF-AM technology. Therefore, the vibration absorption of the LPBF-AMed Ti-6Al 4V alloy may in fact be different from that of alloys fabricated using generally metallurgical fabrication methods such as casting, forging, and rolling [11]. However, studies on the vibration absorption of AMed Ti-6Al-4V alloys are lacking.

In this study, the vibration absorption of a Ti-6Al-4V alloy fabricated using LPBF was evaluated, and the effects of solution treatment followed by water quenching on the vibration absorption of the alloy was investigated.

## 2. Experimental

### 2.1 Specimen preparation

Spherical Ti-6Al-4V powder with a particle diameter of 20 μm to 65 μm (Carpenter Additive) was used in this study. Specimens with dimensions of 25 mm × 25 mm × 25 mm were manufactured using a laser powder bed fusion AM machine (SLM Solutions, GmbH). Settings for the experiment were a preheating temperature for the base plate of 50°C or 200°C, laser power of 300 W, spot diameter of 80 μm, stacking thickness of 50 μm, scanning speed of 775 mm·s$^{-1}$, and hatch pitch of 0.12 mm. Hereafter, depending on the shape and preheating temperature of the base plate, the two specimens are referred to as cube50 and cube200, respectively. Figure 1 shows the scanning and building directions as well as the appearance of the as-built Ti-6Al-4V. The planes perpendicular to the building direction were designated as B1, and those parallel and perpendicular to the scanning direction were designated as A1 and C1, respectively. In addition, those planes facing each other were designated as A2, B2, and C2. The as-built cube50 and cube200 were subjected to solution treatments at 1100°C in an argon atmosphere for 90 min followed by water quenching, as a post-heat treatment.

The microstructures of the specimens were examined using optical microscopy and X-ray diffraction (XRD). The surfaces of the specimens were wet-polished with waterproof abrasive papers up to #2000 and then buff-polished with a colloidal silica suspension to a mirror finish. The mirror-polished surfaces were etched using aqueous solutions of nitric and hydrofluoric acids.

### 2.2 Vibration absorption evaluation

Vibration absorbency was evaluated using a damping method. The specimens were subjected to direct impacts and vibrations. To prevent the specimens from being subjected to other vibrations, the measurement device consisted of two parts, one that supported three eddy current sensors, and the other to hold the specimen. Figure 2 shows a schematic and photograph of the self-developed device for simultaneous multidirectional vibration measurements. To measure the vibration damping caused by the displacement of the specimen, eddy current sensors were installed along the x, y, and z axes perpendicular to the specimen surface. A solenoid was used to apply an impact to the top surface of the specimen, and the specimen was placed on the support to which a vibration-absorbing material made of ABS resin was attached. The vibration-absorbing material was placed in contact with five surfaces, excluding the top surface where the impact was applied. The support was a hollow conical component designed so that the eddy current sensor could be placed inside. Strain gauges were mounted at four locations on the outer frame of the device, and their strain values were maintained at less than 70 με during the measurement. The voltage values received from the transducer were converted into digital signals using an analog-to-digital converter, and a vibration-damping graph was generated on a PC. The damping periods of the specimens were extracted from this graph. Because the specimens were subjected to a mixture of various vibrations, Fourier analysis was applied to extract only the vibration data. Analysis was then performed using Origin2021 software to obtain the frequencies and amplitudes, and the logarithmic damping rate was derived using the damping method. Figure 3 shows the vibration measurement directions. The logarithmic damping rates in the A1A2, B1B2, and C1C2 directions were measured, and the vibration absorbency in each direction was evaluated for the as-built and post-heat-treated specimens.

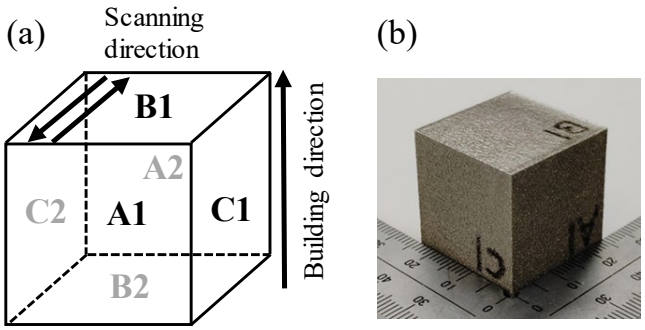


**Figure 1.** (a) Scanning and building directions and (b) appearance of the as-built cube50 specimen.

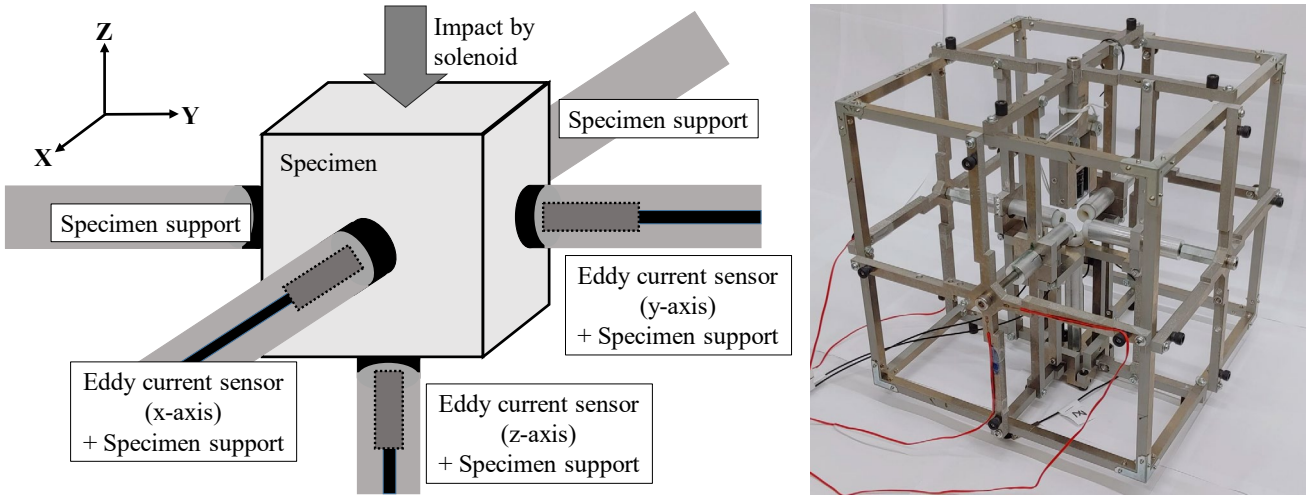


**Figure 2.** Schematic and appearance of the developed device for simultaneous multi-directional vibration measurements.

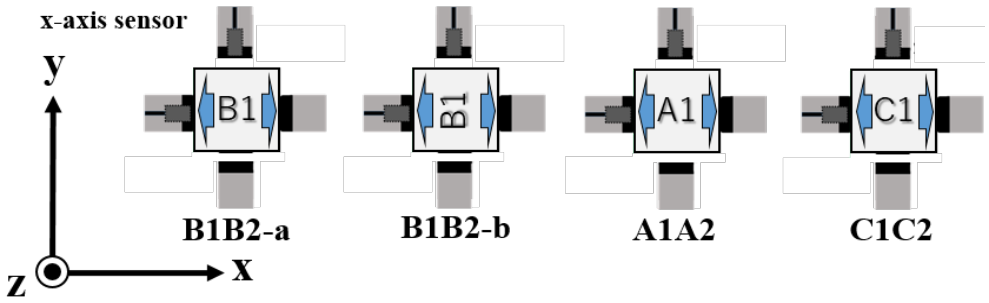


**Figure 3.** Vibration measurement directions using the developed device.

## 3. Results and discussion

Figure 4 presents optical micrographs of the A1, B1, and C1 planes of the as-built specimens under different base-plate temperatures. On the A1 plane, although traces of U-shaped melt-pool boundaries were observed in both the as-built cube50 and cube200 specimens, the stacking interval of solidified melt pool was shorter at a preheating temperature of 200°C than at 50°C. Similarly, a shorter stacking interval was observed for the as-built cube200 than for cube50 on the C1 plane. However, practically no difference was observed in the solidification morphology of the melt pool in the as-built cube200 and cube50 on the B1 plane. According to the literature, the base-plate preheating temperature is related to melt pool geometry. Higher preheating temperature induces deeper and wider melt pools as well as low cooling rates [12]. However, if the stacking thickness during manufacturing is constant, although the depth of melt pool is different, the stacking interval of solidified melt pool should also be constant. Therefore, it is considered that the height of solidified melt pool was changed by different preheating temperature of base plate and then higher preheating temperature leaded to be lower solidified melt pool in height. In fact, it has been reported that higher preheating temperature reduced the contact angle of solidified melt pool track [13]. The smaller the contact angle was, the lower the height of solidified melt pool track was [14].

Figure 5 shows the optical micrographs of the A1 planes of the as-built and post-heat-treated specimens under different base-plate temperatures. Following post-heat treatment, equiaxed grains were observed in both cube200 and cube50. In addition, the acicular phase appeared as martensite inside the equiaxed grains of the post-heat-treated cube200 and cube50.

Figure 6 shows the XRD profiles of the A1 planes inside the as-built and post-heat-treated cube50. In the as-built cube50, the hcp phase was detected, but bcc phase was not. In contrast, not only the hcp phase but also bcc phase was detected in the post-heat-treated cube50. Further, the peaks of hcp phase were shifted slightly and became sharper by post-heat-treatment. The bcc phase can be identified as β phase, but hcp phase is possible to be α or α' martensite. Matsumoto *et al.* have reported that the broad peaks and peak splitting of hcp reflections could be observed by XRD and corresponding to coexistence of α and α' martensite in Ti-6Al-4V alloy quenched from 1223 K, which is a temperature just below β transus at 1268 K [15]. Moreover, Kaschel *et al.* have indicated by In-situ XRD that the splitting of $(0002)_\alpha$ peak occurs when the onset of β phase formation and α' martensite decomposition is demonstrated [16]. They have proposed that this peak splitting is derived from the variation of c/a ratio of hcp lattice due to the alloying element partitioning. The c/a ratios of α' martensite in the as-built specimen and of α in the annealed specimen (after the in-situ XRD) for a LPBF-AMed Ti-6Al-4V alloy have been reported to be 1.588476 and 1.620643, respectively. According to these reportes, the decomposition from α' martensite to α and β phases occurred probably during cooling in this study because the specimens were relatively large and thus the cooling rate inside was not sufficient for α' martensite formation despite water quenching. Therefore, the as-built cube200 and cube50 overall consisted of α and/or α' martensite, but α' martensite near surface and α and β phases inside formed for the post-heat-treated cube200 and cube50.

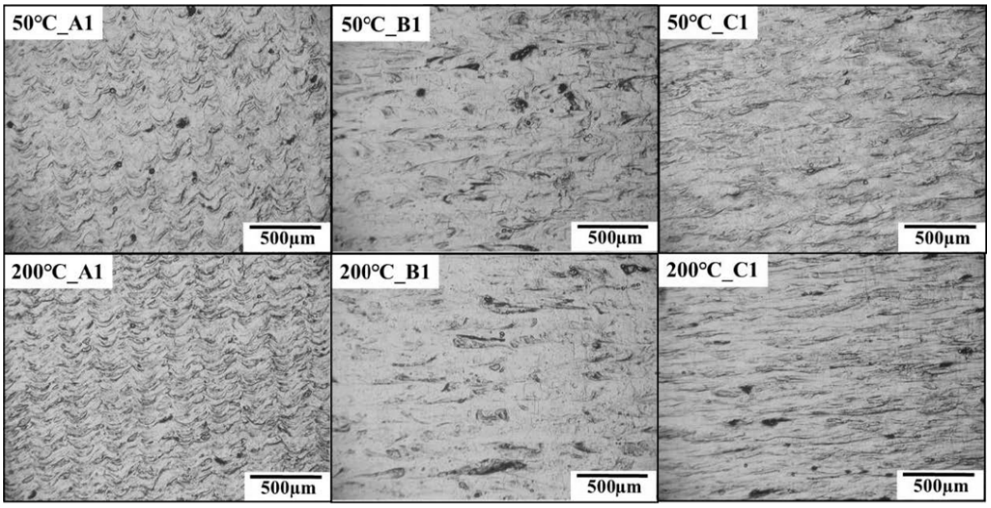


**Figure 4.** Optical micrographs of A1, B1, and C1 planes of the as-built Ti-6Al-4V alloy specimens under different base-plate temperatures.

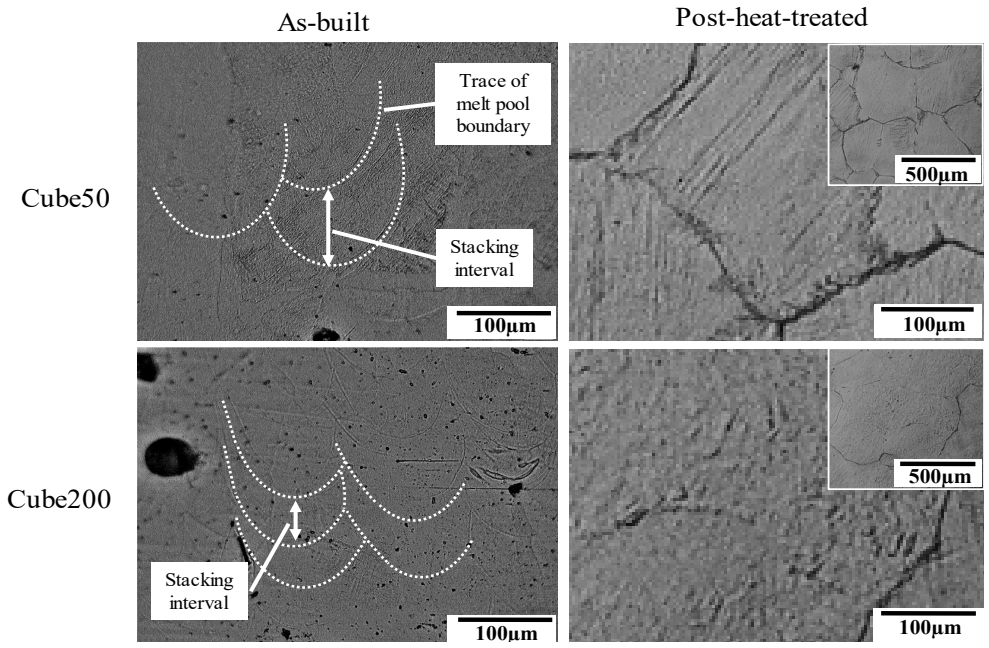


**Figure 5.** Optical micrographs of A1 planes of the as-built and post-heat-treated Ti-6Al-4V alloy specimens under different base-plate temperatures

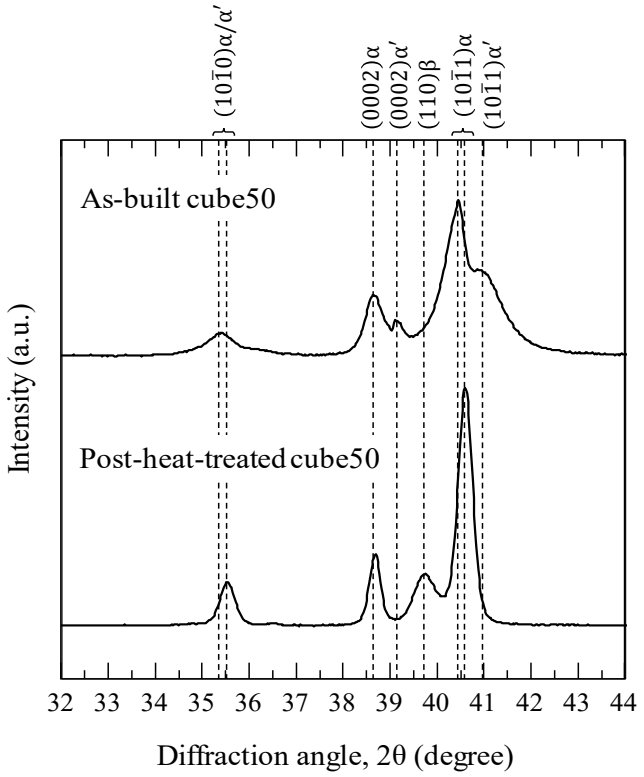


**Figure 6.** XRD profiles of A1 planes inside the as-built and post-heat-treated Ti-6Al-4V alloy specimens (cube50) under different base-plate temperatures.

Figure 7 shows the logarithmic damping rates of the as-built and post-heat-treated specimens. For the as-built cube50 and cube200, large differences were observed in the logarithmic damping rates depending on the direction of the measurement. For both specimens, the highest value was obtained in the C1C2 direction followed by the A1A2 direction, and the lowest values were obtained in the B1B2-a and B1B2-b directions. In terms of the effects of the preheating temperatures of the base plate, the values of the as-built cube50 tended to be higher than those of the as-built cube200 in all directions. By contrast, the logarithmic damping rates for the post-heat-treated cube50 and cube200 were nearly the same and independent of the direction of measurement and preheating temperature. In addition, the values were higher in all measurement directions except for the C1C2 direction for the as-built cube50. Results showed that the post-heat treatment could increase the vibration absorption of specimens to a high level and cause them to become isotropic.

Figure 8 shows a schematic of the possible origin of the vibration-absorption anisotropy of the as-built specimens. Because of the temperature difference between the inside and outside the melt pool, solidification began at the melt-pool boundary, and crystal growth occurred toward the inside. During the solidification and subsequent cooling of Ti-6Al-4V alloy, β phase is firstly crystalized in liquid before the α or α' phase formation because of the stable phase at higher temperature. Cubic crystal grains grow in the opposite direction of heat flow during solidification, being preferentially aligned along the $<100>_{\beta}$ orientation [17]. Therefore, depending on the building condition, the β phase is possible to have a strong crystallographic texture along its growth [18,19]. However, the crystal orientation of α' phase which originates from the parent β grains during cooling exhibits the Burgers orientation relationship and all 12 variants with almost no preferred variant selection could be observed in a selective laser melted Ti-6AL-4V alloy [18]. This alloy is an α+β-type alloy with higher α stability and thus the volume fraction of α or α' phase is very high. Therefore, it is considered that the strong vibration-absorption anisotropy of the as-built specimens is not caused by crystallographic texture in this study. Other possibility of factor causing vibration-absorption anisotropy of the as-built specimens is an inherent microstructure consisting of α' martensite such as distribution, density, size etc., relating to a rapid cooling and multiple reheating/cooling cycles. The lower the preheating temperature of the base plate during manufacturing, the greater was the temperature gradient at the boundary of the melt pool. A previous

study reported that the preheating temperature affects the phase constitution of as-built Ti-6Al-4V alloy fabricated by LPBF. The α+β microstructures tended to be formed when the preheating temperature was set to be at 200°C [20]. Therefore, the amount of α' martensite was probably larger for as-built cube50 than cube200. Further, due to the layer-by-layer deposition in LPBF process, as a new layer is deposited, the primary α' martensite is formed in the melt pool during cooling after solidification and a narrow region close to the melt pool boundary reaches temperatures above the β-transus temperature of Ti-6Al-4V alloy so that the primary α' martensite formed in the preceding solidified layer transforms to the β phase. Then, as the laser beam moves away, this β phase transforms to the secondary α' martensite under a rapid cooling condition. Moreover, the region where the secondary α' martensite formed is reheated and such the heat affected regions result in the tertiary α' martensite formation [10]. The size of primary α' martensite including high density of dislocation is larger, while the secondary α' martensite is twinned on fine scale and the tertiary α' martensite is further finer phase [9]. Namely, the microstructures consisting of α' martensite inside and near boundary of melt pool are possibly different. On the other hand, the α' martensite is unstable above 200°C but the decomposition is very limited below 600°C. However, once the temperature is above 900°C, the α' martensite forms again during a rapid cooling. When the thermal cycle of preceding solidified layer is adjusted to a certain temperature range from 600°C to 800°C, the α' martensite decomposition occurs during LPBF process [21]. Further, it has been reported that the temperature variation of Ti-6Al-4V alloy specimen was measured and recorded by thermocouples at three measuring locations (start, middle, and end points of the laser track) during the direct material deposition process. The temperature of specimen at the middle point was higher than those at the start and end points during the cooling cycle, due to the different heat dissipation condition [22]. The heat dissipation condition was poor at the middle point, which was surrounded by Ti-6Al-4V alloy with low thermal conductivity. The preheating temperature of 200°C rather than that of 50°C is likely to decompose or not to form the α' martensite due to the reduced temperature gradient in this study. Similar microstructural evolution (decomposition to α+β phases) is also likely to occur at the center part of specimens due to heat accumulation. According to the above discussion, because heat accumulation is easy to occur inside than near surface of the specimen during LPBF process, the α' martensite is considered more likely to decompose at the bottom of the melt pool than at its side by the thermal cycles. The α' martensite is then distributed continuously at the side of the melt pool along the building direction. However, the experimental results are not enough for this proposed origin of the vibration-absorption anisotropy of the as-built specimens. The microstructural detail will be investigated more deeply in future.

The mechanisms of vibration damping in metallic materials are classified into composite, dislocation, ferromagnetic, and twinning types, depending on their microstructural characteristics [23]. In this study, the effects of defects such as twinning interfaces and dislocations formed in association with martensitic transformation, as in Ti-Nb binary alloys [7,8] increase the internal friction and vibration absorption. On the plane perpendicular to the C1C2 direction, where the vibration absorption was the highest, a successive region covered with the α' martensite at the side of the melt-pool boundary may have formed. This region was sandwiched multiple times to form a mille-feuille-like structure, playing effectively the role in damping vibration. The distance between them is longer for the as-built cube200 than for the as-built cube50 because the width of melt pool is larger as shown in Figure 4. By contrast, the occupancy of α' martensite in the planes perpendicular to the B1B2 and A1A2 directions, where the vibration absorption was low, was lower than that in the plane perpendicular to the C1C2 direction. Therefore, the vibration absorbency is higher for the as-built cube50 than the as-built cube200.

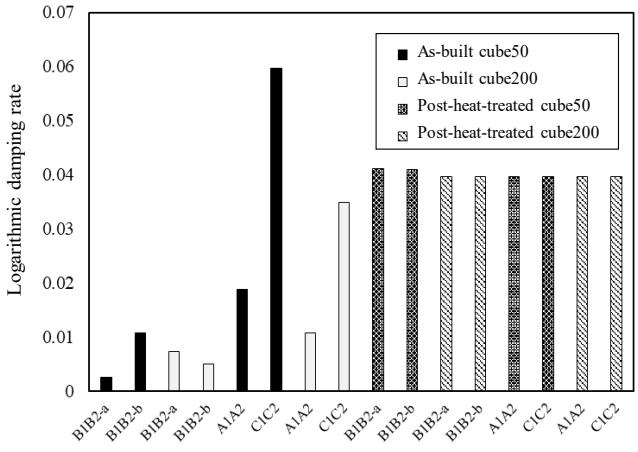


**Figure 7.** Logarithmic damping rates of the as-built and post-heat-treated Ti-6Al-4V alloy specimens.

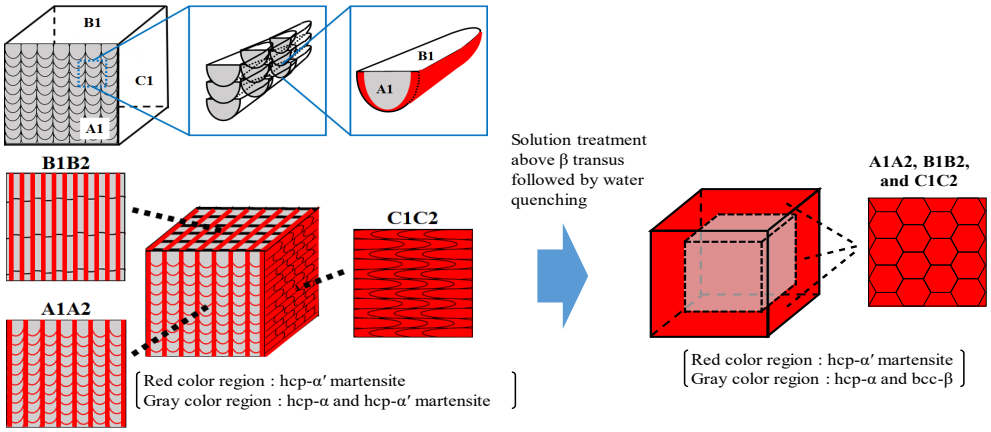


**Figure 8.** Schematic of a possible origin of vibration absorption anisotropy caused by microstructure of the as-built Ti-6Al-4V alloy specimens.

In the post-heat-treated cube50 and cube200, the vibration absorption was nearly equal in all directions. This was attributed to the isotropic distribution of α' martensite with respect to the surface formed in the specimen by solution treatment followed by water quenching. In addition, the post-heat treatment significantly increased the vibration absorbency in all directions, excluding the C1C2 direction of the cube50. This result could be attributed to an increase in the amount of α' martensite in the plane perpendicular to the vibration direction, although decreasing it in the C1C2 direction due to the decomposition to α and β phases inside the specimen.

## 4. Conclusion

This study evaluated the vibration absorption of a Ti-6Al-4V alloy fabricated using LPBF, which is a representative AM technology for metals. The effect of solution treatment followed by water quenching on its vibration absorption was then investigated. The following results were obtained:

1) The vibration absorption of as-built Ti-6Al-4V alloy under a base-plate temperature of 50°C was higher than that under 200°C.

2) Martensite distribution may have been localized near the side of the melt pool in the as-built Ti-6Al-4V alloy, resulting in strong anisotropic vibration absorption.

3) Following post-heat treatment (solution treatment followed by water quenching), martensite was isotropically distributed with respect to the specimen surface of the Ti-6Al-4V alloy such that the anisotropy of vibration absorption was drastically reduced, and high vibration absorption was obtained in all directions.

## Acknowledgment

This study was supported in part by JSPS KAKENHI Grant No. JP20H03595, JIMM Frontier Research Grant, and the fund for Education and Research from the Light Metal Educational Foundation, Inc., Japan.

## References

[1] D. Herzog, V. Seyda, E. Wycisk, and C. Emmelmann, "Additive manufacturing of metals," *Acta Materialia*, vol. 117, pp. 371-392, 2016.

[2] H. Ikeda, and T. Masuoka, "Application of the metal additive manufacturing technology for space vehicle," *Journal of the Japan Society of Precision Engineering*, vol. 82, pp. 639-642, 2016.

[3] J. Fujimoto, "Damping materials for spacecraft structures", *The Journal of the INCE of Japan*, vol. 15, pp. 45-49, 1991.

[4] K. Yoshida, H. Seko, H. Sasano, Q. Shi, and S. Ando, "Acoustically induced random vibration analysis system for artificial satellite," *Mitsubishi Denki Giho*, vol. 85, pp. 390-392, 2011.

[5] S. Asano, and K. Ishii, "Internal Friction of Metals (2)," *Denkiseiko*, vol. 39, pp. 180-191, 1968.

[6] K. Kawahara, and F. Yin, "New type of damping materials, M2052 alloys," *Journal of the Vacuum Society of Japan*, vol. 42, pp.11-17, 1999.

[7] Y. Mantani, T. Tsumura, and K. Nakata, "Effect of α' martensite structure of Ti-15Nb alloy on material properties and its surface hardening treatment by plasma nitriding," *Journal of the Japan society for heat treatment*, vol. 52, pp. 263-268, 2012.

[8] Y. Mantani, and Y. Takemoto, "Change in crystal structure and material properties with deformation of quenched martensite in Ti-Nb alloys," *Journal of the Japan Institute of Metals and Materials*, vol. 79, pp. 461-467, 2015.

[9] J. Yang, H. Yu, J. Yin, M. Gao, Z. Wang, and X. Zeng, "Formation and control of martensite in Ti-6Al-4V alloy produced by selective laser melting," *Materials and Design*, vol. 108, pp. 308-318, 2016.

[10] J. J. S. Dilip, S. Zhang, C. Teng, K. Zeng, C. Robinson, D. Pal, and B. Stucker, "Influence of processing parameters on the evolution of melt pool, porosity, and microstructures in Ti-6Al-4V alloy parts fabricated by selective laser melting," *Progress in Additive Manufacturing*, vol. 2, pp. 157-167, 2017.

[11] X. J. Jiang, S. J. Bao, L. W. Zhang, X. Y. Zhang, L. S. Jiao, H. B. Qi, and F. Wang, "Effect of Zr on microstructure and properties of TC4 alloy fabricated by laser additive manufacturing," *Journal of Materials Research and Technology*, vol. 24, pp. 8782-8792, 2023.

[12] P. Köhnen, M. Létang, M. Voshage, J. H. Schleifenbaum, and C. Haase, "Understanding the process-microstructure correlations for tailoring the mechanical properties of L-PBF produced austenitic advanced high strength steel," *Additive Manufacturing*, vol.30, no. 100914, 2019.

[13] I. Yadroitsev, P. Krakhmalev, I. Yadroitsava, S. Johansson, and I. Smurov, "Energy input effect on morphology and microstructure of selective laser melting single track from metallic powder," *Journal of Materials Processing Technology*, vol. 213, pp. 606-613, 2013.

[14] X. Shi, C. Yan, W. Feng, Y. Zhang. and Z. Leng, "Effect of high layer thickness on surface quality and defect behavior of Ti-6Al-4V fabricated by selective laser melting," *Optics and Laser Technology*, vol. 132, no. 106471, 2020.

[15] H. Matsumoto, H. Yoneda, K. Sato, S. Kurosu, E. Maire, D. Fabregue, T. J. Konno, and A. Chiba, "Room-temperature ductility of Ti–6Al–4V alloy with α' martensitemicrostructure," *Materials Science and Engineering A*, vol. 528, pp. 1512-1520, 2011.

[16] F. R. Kaschel, R. K. Vijayaraghavan, A. Shmeliov, E. K. McCarthy, M. Canavan, P. J. McNally, D. P. Dowling, V. Nicolosi, and M. Celikin, "Mechanism of stress relaxation and phase transformation in additively manufactured Ti-6Al-4V via in situ high temperature XRD and TEM analyses," *Acta Materialia,* vol. 188, pp. 720-732, 2020.

[17] T. Ishimoto, and T. Nakano, "Review-Microstructural control and functional enhancement of light metal materials via metal additive manufacturing," *Materials Transactions*, vol. 64, pp. 10-16, 2023.

[18] M. Simonelli, Y. Y. Tse, and C. Tuck, "On the texture formation of selective laser melted Ti-6Al-4V," Metallurgical and *Materials Transactions A*, vol. 45, pp. 2863–2872, 2014.

[19] H. Amano, T. Ishimoto, R. Suganuma, K. Aiba, S. Sun, R. Ozasa, and T. Nakano, "Effect of a helium gas atmosphere on the

mechanical properties of Ti-6Al-4V alloy built with laser powder bed fusion: A comparative study with argon gas," *Additive Manufacturing*, vol. 48, no. 102444, 2021.

[20] S. Cao, Y. Zou, C.V.S. Lim, and X. Wu, "Review of laser powder bed fusion (LPBF) fabricated Ti-6Al-4V: process, post-process treatment, microstructure, and property," *Light: Advanced Manufacturing*, vol. 2, pp. 313-332, 2021.

[21] Y. Xu, D. Zhang, Y. Guo, S. Hu, X. Wu, and Y. Jiang, "Micro-structural tailoring of As-Selective Laser Melted Ti6Al4V alloy for high mechanical properties," *Journal of Alloys and Compounds*, vol. 816, no. 152536, 2020.

[22] S. Li, B. Zhang, and Q. Bai, "Effect of temperature buildup on milling forces in additive/subtractive hybrid manufacturing of Ti-6Al-4V," *The International Journal of Advanced Manufacturing Technology*, vol. 107, pp. 4191-4200, 2020.

[23] Y. Mae, ""Damping mechanism and its characteristics of damping alloys," *Journal of the Japan Society of Precision Engineering*, vol. 55, pp. 2123-2126, 1989.